



## An Integrated Framework for Geothermal Energy Storage with CO<sub>2</sub> Sequestration and Utilization

Liu, Yueliang; Hu, Ting; Rui, Zhenhua; Zhang, Zheng; Du, Kai; Yang, Tao; Dindoruk, Birol; Halfdan Stenby, Erling; Torabi, Farshid; Afanasyev, Andrey

*Published in:*  
Engineering

*Link to article, DOI:*  
[10.1016/j.eng.2022.12.010](https://doi.org/10.1016/j.eng.2022.12.010)

*Publication date:*  
2024

*Document Version*  
Publisher's PDF, also known as Version of record

[Link back to DTU Orbit](#)

*Citation (APA):*  
Liu, Y., Hu, T., Rui, Z., Zhang, Z., Du, K., Yang, T., Dindoruk, B., Halfdan Stenby, E., Torabi, F., & Afanasyev, A. (2024). An Integrated Framework for Geothermal Energy Storage with CO<sub>2</sub> Sequestration and Utilization. *Engineering*, 30, 121-130. <https://doi.org/10.1016/j.eng.2022.12.010>

---

### General rights

Copyright and moral rights for the publications made accessible in the public portal are retained by the authors and/or other copyright owners and it is a condition of accessing publications that users recognise and abide by the legal requirements associated with these rights.

- Users may download and print one copy of any publication from the public portal for the purpose of private study or research.
- You may not further distribute the material or use it for any profit-making activity or commercial gain
- You may freely distribute the URL identifying the publication in the public portal

If you believe that this document breaches copyright please contact us providing details, and we will remove access to the work immediately and investigate your claim.



## Research Large-Scale Energy Storage—Article

# An Integrated Framework for Geothermal Energy Storage with CO<sub>2</sub> Sequestration and Utilization



Yueliang Liu<sup>a,b,c,#</sup>, Ting Hu<sup>b,#</sup>, Zhenhua Rui<sup>a,b,c,\*</sup>, Zheng Zhang<sup>b</sup>, Kai Du<sup>b</sup>, Tao Yang<sup>d</sup>, Birol Dindoruk<sup>e</sup>, Erling Halfdan Stenby<sup>f</sup>, Farshid Torabi<sup>g</sup>, Andrey Afanasyev<sup>h</sup>

<sup>a</sup> State Key Laboratory of Petroleum Resources and Prospecting, China University of Petroleum (Beijing), Beijing 102249, China

<sup>b</sup> School of Petroleum Engineering, China University of Petroleum (Beijing), Beijing 102249, China

<sup>c</sup> College of Carbon Neutrality Future Technology, China University of Petroleum (Beijing), Beijing 102249, China

<sup>d</sup> Equinor ASA, Stavanger 4035, Norway

<sup>e</sup> Department of Petroleum Engineering, Cullen College of Engineering, University of Houston, Houston, TX 77204, USA

<sup>f</sup> Center for Energy and Resources Engineering, Department of Chemistry, Technical University of Denmark, Kongens Lyngby 2800, Denmark

<sup>g</sup> Petroleum Systems Engineering, University of Regina, Regina, SK S4S 0A2, Canada

<sup>h</sup> Institute of Mechanics, Moscow State University, Moscow 119192, Russia

## ARTICLE INFO

### Article history:

Received 13 September 2022

Revised 28 November 2022

Accepted 23 December 2022

Available online 8 March 2023

### Keywords:

Geothermal energy storage

CO<sub>2</sub> sequestration

Carbon neutrality

Large-scale

CO<sub>2</sub> utilization

## ABSTRACT

Subsurface geothermal energy storage has greater potential than other energy storage strategies in terms of capacity scale and time duration. Carbon dioxide (CO<sub>2</sub>) is regarded as a potential medium for energy storage due to its superior thermal properties. Moreover, the use of CO<sub>2</sub> plumes for geothermal energy storage mitigates the greenhouse effect by storing CO<sub>2</sub> in geological bodies. In this work, an integrated framework is proposed for synergistic geothermal energy storage and CO<sub>2</sub> sequestration and utilization. Within this framework, CO<sub>2</sub> is first injected into geothermal layers for energy accumulation. The resultant high-energy CO<sub>2</sub> is then introduced into a target oil reservoir for CO<sub>2</sub> utilization and geothermal energy storage. As a result, CO<sub>2</sub> is sequestered in the geological oil reservoir body. The results show that, as high-energy CO<sub>2</sub> is injected, the average temperature of the whole target reservoir is greatly increased. With the assistance of geothermal energy, the geological utilization efficiency of CO<sub>2</sub> is higher, resulting in a 10.1% increase in oil displacement efficiency. According to a storage-potential assessment of the simulated CO<sub>2</sub> site, 110 years after the CO<sub>2</sub> injection, the utilization efficiency of the geological body will be as high as 91.2%, and the final injection quantity of the CO<sub>2</sub> in the site will be as high as  $9.529 \times 10^8$  t. After 1000 years sequestration, the supercritical phase dominates in CO<sub>2</sub> sequestration, followed by the liquid phase and then the mineralized phase. In addition, CO<sub>2</sub> sequestration accounting for dissolution trapping increases significantly due to the presence of residual oil. More importantly, CO<sub>2</sub> exhibits excellent performance in storing geothermal energy on a large scale; for example, the total energy stored in the studied geological body can provide the yearly energy supply for over  $3.5 \times 10^7$  normal households. Application of this integrated approach holds great significance for large-scale geothermal energy storage and the achievement of carbon neutrality.

© 2023 THE AUTHORS. Published by Elsevier LTD on behalf of Chinese Academy of Engineering and Higher Education Press Limited Company. This is an open access article under the CC BY license (<http://creativecommons.org/licenses/by/4.0/>).

## 1. Introduction

The atmospheric concentration of carbon dioxide (CO<sub>2</sub>) is increasing sharply due to the acceleration of global industrialization in recent years. This increasing CO<sub>2</sub> concentration is the main

cause of climate change and other deleterious impacts on our living environment [1]. According to the International Energy Agency (IEA) report, global energy-related carbon dioxide emissions increased by 6% to  $3.63 \times 10^{10}$  t in 2021 [2]. The absolute increase in global carbon dioxide emissions exceeded  $2 \times 10^9$  t, the largest increase in history [2].

Since 2000, CO<sub>2</sub> has been used as an excellent working fluid for extracting geothermal energy from deep geothermal layers [3]. Compared with underground brine, CO<sub>2</sub> has three main

\* Corresponding author.

E-mail address: [zhenhuarui@gmail.com](mailto:zhenhuarui@gmail.com) (Z. Rui).

# These authors contributed equally to this work.

superiorities: ① The mineral solubility of  $\text{CO}_2$  is smaller than that of formation brine, which reduces pipe or equipment scaling [3]; ② the kinematic viscosity of  $\text{CO}_2$  is lower than that of formation brine, which reduces the pressure losses to reservoir rocks [4,5]; and ③  $\text{CO}_2$  is more compressible than liquid water, which allows the generation of a thermosiphon, reducing the strict requirement for circulation pumps [6–9]. It has been found that  $\text{CO}_2$  has a higher heat transfer rate than formation brine [10]. However, the geothermal layers have their limited potential for  $\text{CO}_2$  storage due to its limited reservoir volume for sequestration [11,12]. Therefore, sedimentary geothermal basins with extremely low permeability caprocks have been proposed for  $\text{CO}_2$  storage, as they have been recognized to have large potential for this purpose [13–17]. Recently, the depleted natural gas reservoirs [18] and depleted oil reservoirs [19] was proposed for the suitable sites for  $\text{CO}_2$  sequestration and energy storage [20].

Fossil fuel burning generates significant  $\text{CO}_2$  emissions, accounting for 73% of global carbon emissions [21].  $\text{CO}_2$  utilization and storage are currently regarded as one of the most feasible and applicable  $\text{CO}_2$  capture, utilization, and storage (CCUS) technologies, accounting for 77% of total global carbon reduction to date [22]. One of the most promising methods of  $\text{CO}_2$  utilization and storage is to simultaneously use enhanced oil recovery combined with  $\text{CO}_2$  sequestration in target reservoirs [23–28]. The performance of  $\text{CO}_2$  in enhanced oil recovery greatly relies on the mass transfer between  $\text{CO}_2$  and crude oil [29–34]. It has been found that miscibility or near-miscibility achieves higher oil recovery than immiscibility [35–38]. In addition, the  $\text{CO}_2$  storage potential is more significant under the condition of miscibility or near-miscibility than under immiscibility [35–38]. To achieve miscibility, the system pressure should be at or above the minimum miscibility pressure (MMP) [39]. However, it is uneconomical to increase the target reservoir pressure artificially to achieve miscibility [40,41]. Recently, chemical solvents such as alcohol, propanol, and dimethyl ether [42,43] have been introduced to accompany  $\text{CO}_2$  in enhanced oil recovery, reducing the MMP between  $\text{CO}_2$  and crude oil by more than 10%. In addition to reduc-

ing the MMP, modified  $\text{CO}_2$  injection—such as water alternating gas (WAG) and so forth—has been investigated in order to improve the  $\text{CO}_2$  injection performance by increasing the sweep efficiency of  $\text{CO}_2$  [44–49].

In this work, we propose an integrated framework for synergistic geothermal energy storage and  $\text{CO}_2$  sequestration and utilization. Within this framework,  $\text{CO}_2$  is first injected into geothermal layers, where the geothermal energy is efficiently transferred to the low-temperature  $\text{CO}_2$  due to the higher heat transfer coefficient of the latter. The resultant high-energy  $\text{CO}_2$  is then introduced into the target reservoir for simultaneous  $\text{CO}_2$  utilization and sequestration and geothermal energy storage. The schematic work flows of this integrated framework are shown in Fig. 1.

## 2. Theoretical model

### 2.1. Overview of simulation tools

In this work, simulations were performed using the TOUGHREACT-EOR code package, which can simulate the interaction between  $\text{CO}_2$  and multicomponent oil phases, as well as the multicomponent reactive transport of a complex aqueous phase in subsurface multiphase systems. This simulator has been updated by introducing a multicomponent oil phase to the existing simulation framework of multiphase flow and heat flow with reactive transport [50–52]. For numerical calculations, spatial discretization was carried out using the integral finite difference (IFD), and the time discretization was the fully implicit difference. A sequential iterative approach that referred to a previous work [53] was used in the coupled calculation of flow and reactive transport. Details on the reactive transport simulator are provided in a previous work [54].

The updated oil-bearing multiphase, multicomponent simulation program, coupled with a thermo-hydro-chemical (T-H-C) simulator, still possesses all the merits of the original simulator (i.e., non-isothermal, multiphase solute transport considering convection diffusion, geochemical reactions, and a comprehensive

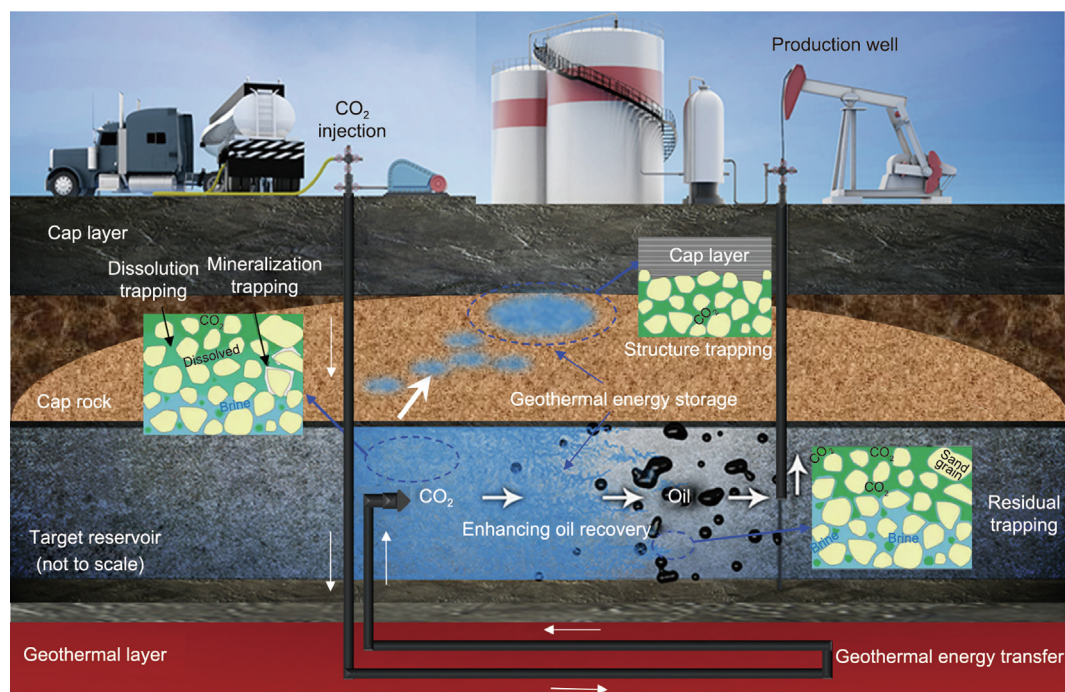


Fig. 1. Schematic work flows of the integrated framework for geothermal energy storage and  $\text{CO}_2$  sequestration and utilization.

database of thermodynamic and kinetic parameters). The key differences are that the updated simulator takes into account the following processes: ① flash evaporation to solve the mass transfer process between CO<sub>2</sub> and the multicomponent oil phase; and ② CO<sub>2</sub> miscibility and immiscibility. Overall, the updated simulator can quantitatively characterize the migration and transformation of CO<sub>2</sub> among the supercritical phase, dissolved-in-water phase, dissolved-in-oil phase, and mineralized phase; thus, it is an optional software for carbon sequestration research in CO<sub>2</sub>-geological utilization technology.

## 2.2. Model initial and boundary conditions

In this study, we developed a three-dimensional (3D) wellbore-reservoir coupling model. Fig. 2 presents the longitudinal section of the wellbore-reservoir coupling model, which uses different governing equations to calculate the fluid phase behavior in the wellbore and reservoir. The one-dimensional (1D) two-phase momentum equation is used for the wellbore and the 3D multi-phase Darcy's Law is employed for the reservoir [55]. The thickness of the entire stratum is 2.02 km, including a geothermal layer located at the bottom, with a thickness of 100 m and a depth of 3.52 km, and an oil reservoir at the top, with a thickness of 20 m and a depth of 1.5 km. A group of injection-production wells in an inverse “nine-point” well pattern is defined in the model to finish the desired simulation work. Based on the symmetry principle, the 1/4 area of the well pattern is simulated and Dirichlet conditions with fixed temperature and pressure are considered for the lateral boundaries. A semi-analytical solution is used to calculate the heat exchange between the wellbore and formation [56].

Fluids are heated in the geothermal formation through a 200 m horizontal well and then injected into the oil reservoir along a 2.0 km long vertical well. Details of the target reservoir's initial

physical parameters and the pseudo components of the crude oil used in our model are provided in Tables 1 and 2 [57], respectively. Details of the geothermal formation's initial physical parameters and the wellbore parameters are presented in Table 3 [58].

The geochemical conditions of the model are set according to the site data. The aqueous solution type is Na–HCO<sub>3</sub>, and the stratigraphic lithology is feldspar quartz sandstone. We consider three mechanisms influencing the kinetically controlled mineral dissolution and precipitation, and the reaction rate constant ( $k$ ) is calculated using the Lasaga model (1984), as shown in Eq. (1):

$$k = k_{25}^{\text{nu}} \exp \left[ \frac{-E_a^{\text{nu}}}{R} \left( \frac{1}{T_0} - \frac{1}{298.15} \right) \right] + k_{25}^{\text{H}} \exp \left[ \frac{-E_a^{\text{H}}}{R} \left( \frac{1}{T_0} - \frac{1}{298.15} \right) \right] \alpha_{\text{H}}^{n_{\text{H}}} + k_{25}^{\text{OH}} \exp \left[ \frac{-E_a^{\text{OH}}}{R} \left( \frac{1}{T_0} - \frac{1}{298.15} \right) \right] \alpha_{\text{OH}}^{n_{\text{OH}}} \quad (1)$$

where  $k_{25}$  (mol·(m<sup>2</sup>·s)<sup>−1</sup>) is the kinetic constant at 25 °C, and  $E_a$  (kJ·mol<sup>−1</sup>) is the activation energy,  $R$  is gas constant,  $T_0$  is absolute temperature (K),  $\alpha$  is the activity of the species. The power terms ( $n$ ) for both the acid (H) and base (OH) mechanisms are for H<sup>+</sup>, superscripts nu indicate neutral mechanisms. The reaction kinetic parameters related to the geochemical calculation are listed in Tables 4 and 5 [59–61].

The solubilities of the CO<sub>2</sub> and the hydrocarbon component in the gas and oil phases are calculated by flash calculations using the Peng–Robinson (PR) equation of state, and the solubility of the CO<sub>2</sub> in the water phase is calculated using Henry's law. The oil viscosity ( $\mu$ ) in our model is considered to be a function of temperature, pressure, the compression coefficient, and the

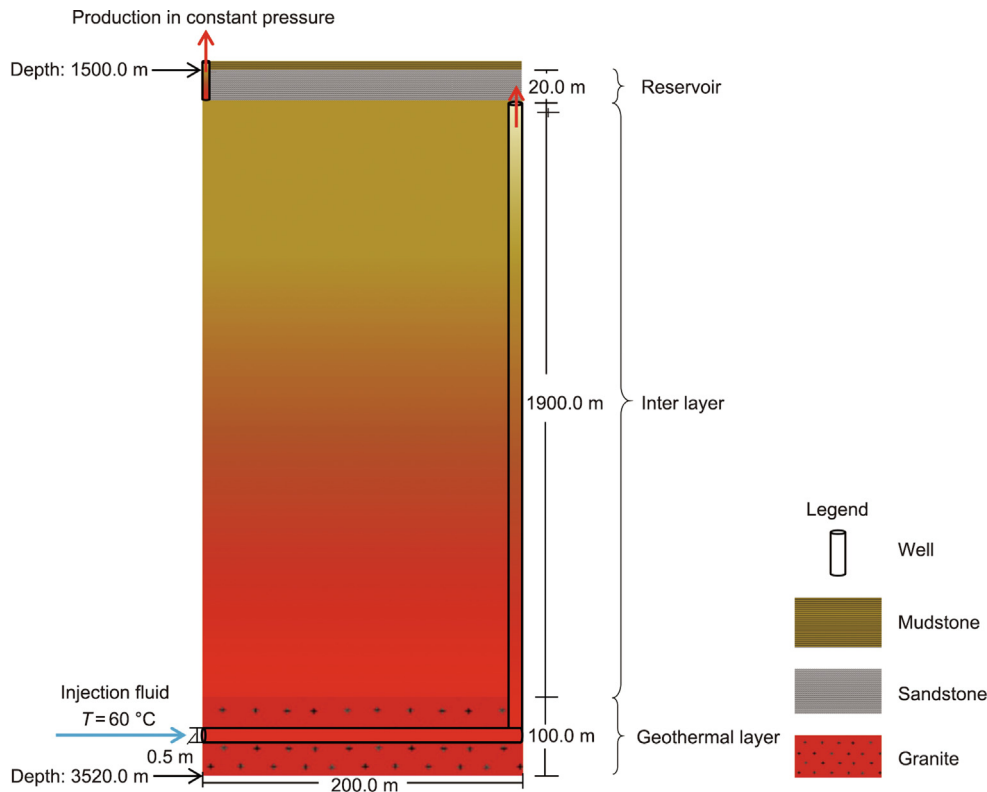


Fig. 2. Longitudinal section of the wellbore-reservoir coupling model.



component properties, taking friction theory into account [62], as shown in Eq. (2):

$$\mu = \frac{1}{f} = \frac{1}{\sum_{i=1}^N \sum_{j=1}^N \frac{\theta_i \theta_j E_{ij}^A}{\sqrt{u_i u_j}}} \quad (2)$$

where  $f$  is the fluidity of multicomponent fluids;  $N$  is the number of components;  $u_i$  and  $u_j$  are the viscosity of components  $i$  and  $j$ , respectively;  $\theta_i$  ( $\theta_j$ ) is the function of  $x_i$  ( $x_j$ ) and  $M_i$  ( $M_j$ ); and  $E_{ij}^A$  is the average efficiency interaction coefficient between component  $i$  and  $j$ , as shown in Eqs. (3)–(5):

$$\mu_i = \mu_c [1 + a(P - P_c)] \exp(E_a/RT) \quad (3)$$

$$\theta_i = \frac{x_i \sqrt{M_i}}{\sum_{i=1}^N x_i M_i} \quad (4)$$

$$E_{ij}^A = \frac{2\sqrt{M_i M_j}}{M_i + M_j} \quad (5)$$

where  $\mu_c$  is the critical viscosity;  $T$  is temperature (K);  $P$  is pressure (Pa);  $a$  is pressure coefficient ( $\text{Pa}^{-1}$ );  $x_i$  is the molar fraction of component  $i$ ; and  $M_i$  and  $M_j$  are the molecular mass of components  $i$  and  $j$ , respectively.

In this work, the target reservoir is developed by alternately injecting CO<sub>2</sub> and water for 10 years. In the first (i.e., 0–2.5 years) and third (i.e., 5.0–7.5 years) periods of 2.5 years, CO<sub>2</sub> injection is performed. In the second (i.e., 2.5–5.0 years) and fourth (i.e., 7.5–10.0 years) periods of 2.5 years, water injection is performed to improve the sweep volume of the injected fluid and enhance the heat transfer capacity of the geothermal layers. After 10 years of alternating injection cycles, CO<sub>2</sub> is injected continuously for 100 years for CO<sub>2</sub> sequestration and geothermal energy storage; here, it should be noted that geothermal energy is stored in the target geological reservoir body accompanying CO<sub>2</sub> sequestration. Three cases are adopted in this simulation: case 1, in which the CO<sub>2</sub> or water is first injected into the geothermal layers for energy assimilation, and the high-energy CO<sub>2</sub> is then injected into the

target geological reservoir body for CO<sub>2</sub> utilization—that is, enhanced oil recovery; case 2, in which CO<sub>2</sub> or water is injected into the target reservoir directly for oil recovery; and case 3, in which the target oil reservoir is assumed to be depleted, and CO<sub>2</sub> is then injected for 100 years for sequestration and, more importantly, geothermal energy is stored in the CO<sub>2</sub> accompanying the CO<sub>2</sub> sequestration.

### 3. Calculation of energy storage with CO<sub>2</sub>

At a given pressure and temperature, the total energy stored in CO<sub>2</sub> is composed of the temperature exergy and the pressure exergy [63], which are given by Eq. (6):

$$e_{x,H} = e_{x,T} + e_{x,P} \quad (6)$$

where  $e_{x,H}$  represents the specific enthalpy (i.e., total energy) of CO<sub>2</sub> under given conditions, in  $\text{kJ}\cdot\text{kg}^{-1}$ ;  $e_{x,T}$  represents the specific exergy to temperature, in  $\text{kJ}\cdot\text{kg}^{-1}$ ; and  $e_{x,P}$  represents the specific exergy to pressure, in  $\text{kJ}\cdot\text{kg}^{-1}$ .

The  $e_{x,P}$  can be considered to be the work done by CO<sub>2</sub> expansion under isothermal conditions, which can be expressed as shown in Eq. (7) [58]:

$$e_{x,P} = e_x(T_s, P_1) - e_x(T_s, P_2) = \int_{P_2}^{P_1} V dP = T_s R_g \ln \frac{P_1}{P_2} \quad (7)$$

where  $e_x$  represents the specific exergy, in  $\text{kJ}\cdot\text{kg}^{-1}$ ;  $T_s$  represents the system temperature, in K;  $P_1$  represents the absolute pressure of CO<sub>2</sub> in the target reservoir, in MPa;  $P_2$  represents the absolute pressure of natural gas at the ground surface, in MPa;  $V$  represents the specific volume of CO<sub>2</sub>, in  $\text{m}^3\cdot\text{kg}^{-1}$ ; and  $R_g$  represents the gas molar constant.

When the temperature is changed from  $T_s$  to the given temperature, the  $e_{x,T}$  is calculated as shown in Eq. (8) [64]:

$$\begin{aligned} e_{x,T} &= e_x(T_1, P_1) - e_x(T_s, P_1) = \int_{T_s}^{T_1} C_p (1 - \frac{T_s}{T_1}) dT \\ &= C_p (T_s - T_1) - C_p T_s \ln \frac{T_s}{T_1} \end{aligned} \quad (8)$$

where  $T_1$  represents the temperature of CO<sub>2</sub>, in K; and  $C_p$  represents the specific heat capacity at the given pressure, in  $\text{kJ}\cdot(\text{kg}\cdot\text{K})^{-1}$ .

## 4. Results and discussion

### 4.1. Improved reservoir temperature

The initial temperature of the target reservoir is 333.15 K. The temperature increment of high-energy CO<sub>2</sub>/water after flowing through the geothermal layer is expressed as follows (Fig. S1 in Appendix A): During the first 2.5 years, CO<sub>2</sub> is injected through the geothermal layer, which has a temperature of 383.15 K, and is then injected into the target reservoir, which has an initial temperature of 333.15 K. The temperature of the high-energy CO<sub>2</sub>

**Table 1**  
Initial parameters of the target oil reservoir.

Parameter (unit)	Value
Density of the reservoir rock ( $\text{kg}\cdot\text{m}^{-3}$ )	2600
Porosity	0.148
Depth of the bottom rock (m)	1500
Permeability (mD)	10.2
Temperature (K)	333.15
Pressure (MPa)	15.0
Heat conduction coefficient of the reservoir rocks ( $\text{J}\cdot(\text{kg}\cdot\text{K})^{-1}$ )	2.51
Specific heat capacity of the reservoir rocks ( $\text{W}\cdot(\text{m}\cdot\text{K})^{-1}$ )	920
Thickness of reservoir (m)	20.0
Oil saturation	0.51

**Table 2**  
Initial pseudo-components of the target reservoir fluid [57].

Component	Mole fraction	$P_c$ (atm <sup>a</sup> )	$T_c$ (K)	$V_c$ ( $\text{cm}^3\cdot\text{mol}^{-1}$ )	Molecular weight ( $\text{g}\cdot\text{mol}^{-1}$ )	Acentric factor
CO <sub>2</sub>	0.00970	72.900	304.700	0.094000	44.010	0.225000
N <sub>2</sub> and C <sub>1</sub>	0.30880	45.158	189.078	0.089500	16.326	0.013638
C <sub>2</sub>	0.03960	48.200	305.430	0.009000	30.070	0.098600
C <sub>3</sub> and C <sub>4</sub>	0.04660	40.703	382.490	0.148000	47.589	0.163450
i-C <sub>5</sub> and C <sub>6</sub>	0.00170	32.909	470.810	0.203000	73.545	0.248180
C <sub>7</sub> –C <sub>10</sub>	0.05370	26.390	595.870	0.255780	118.180	0.343530
C <sub>11</sub> –C <sub>25</sub>	0.16197	19.357	617.830	0.327352	175.470	0.822800
C <sub>25+</sub>	0.37790	16.922	907.900	0.442394	534.800	1.151000

$P_c$ : the critical pressure;  $T_c$ : the critical temperature;  $V_c$ : the critical volume; i-C<sub>5</sub>: isopentane.

<sup>a</sup> 1 atm = 101325 Pa.

**Table 3**

List of thermo-physical parameters of the deep geothermal layer.

Parameter (unit)	Value
Density of reservoir rock ( $\text{kg}\cdot\text{m}^{-3}$ )	2600
Porosity	0.148
Permeability (mD)	0.101
Depth of bottom rock (m)	3000
Temperature of bottom rock (K)	383.15
Heat conduction coefficient of reservoir rocks ( $\text{J}\cdot(\text{kg}\cdot\text{K})^{-1}$ )	2.51
Specific heat capacity of reservoir rocks ( $\text{W}\cdot(\text{m}\cdot\text{K})^{-1}$ )	920
Heat conduction coefficient of well wall ( $\text{J}\cdot(\text{kg}\cdot\text{K})^{-1}$ )	Horizontal: 4.00, vertical: 0.02
Specific heat capacity of well wall ( $\text{W}\cdot(\text{m}\cdot\text{K})^{-1}$ )	750
Diameters of tube (m)	0.5

**Table 4**

Initial water chemical composition [59].

Component	C ( $\text{mol}\cdot\text{L}^{-1}$ )	Component	C ( $\text{mol}\cdot\text{L}^{-1}$ )
$\text{Na}^+$	$9.25 \times 10^{-2}$	$\text{SO}_4^{2-}$	$1.09 \times 10^{-2}$
$\text{K}^+$	$2.88 \times 10^{-2}$	$\text{HCO}_3^-$	$3.37 \times 10^{-2}$
$\text{Ca}^{2+}$	$1.26 \times 10^{-3}$	$\text{Cl}^-$	$1.26 \times 10^{-1}$
$\text{Mg}^{2+}$	$1.17 \times 10^{-3}$	—	—

C: total dissolved concentrations of chemical components, which are concentrations of the basis species plus their associated aqueous secondary species.

(which averages 341.75 K) is always higher than the initial reservoir temperature (333.15 K). To improve the utilization efficiency of the  $\text{CO}_2$ , its injection is alternated with water injection in the second 2.5-year period. It can be seen that the temperature of the injected water is higher than that of the  $\text{CO}_2$ , reaching as high as 355.45 K, because the specific heat capacity per unit mass of water is higher than that of  $\text{CO}_2$ .

In the third period of 2.5 years, high-energy  $\text{CO}_2$  is reinjected into the target reservoir. As shown in Fig. S1, the temperature of the high-energy  $\text{CO}_2$  decreases sharply at the beginning of the injection. After 2.5 years of water injection, condensate water has filled in the wellbore at the section between the geothermal layer and the target reservoir. When the high-energy  $\text{CO}_2$  flows through this section, substantial heat loss occurs due to heat exchange with the condensate water, resulting in an intense decrease in the tem-

perature of the high-energy  $\text{CO}_2$ . However, the temperature of the high-energy  $\text{CO}_2$  gradually increases to around 341.15 K, which is deemed to be beneficial for  $\text{CO}_2$  utilization. In the fourth 2.5-year period, water is again injected, this time with an average temperature as high as 351.15 K, which is much higher than the original target reservoir temperature of 333.15 K.

The temperature distributions over the target reservoir during the two cycles of  $\text{CO}_2$ /water injection are shown in Appendix Fig. S2. The temperature around the injecting wellbore for the high-energy  $\text{CO}_2$ /water injection is much higher than that of the main body of the target reservoir. Compared with the high-energy  $\text{CO}_2$  injection, the high-energy water injection results in a much higher temperature around the injection wellbore. The average temperature of the target reservoir during the 0–2.5-year and 5.0–7.5-year periods of high-energy  $\text{CO}_2$  injection is 335.4 and 336.41 K, respectively, which is higher than the initial temperature of the target reservoir. Moreover, the average temperature of the target reservoir during the 2.5–5.0-year and 7.5–10.0-year periods of high-energy water injection is 336.9 and 338.23 K, respectively; thus, the high-energy water injection better promotes the target reservoir temperature than the high-energy  $\text{CO}_2$  injection. Compared with injecting  $\text{CO}_2$ /water directly, the high-energy  $\text{CO}_2$ /water injection results in the target reservoir having relatively higher temperatures. Higher temperatures enhance the transfer of  $\text{CO}_2$  to crude oil and reduce the oil's viscosity, which result in a higher efficiency of  $\text{CO}_2$  utilization for enhanced oil recovery. Furthermore, a higher temperature is critical for large-scale geothermal energy storage in  $\text{CO}_2$ .

#### 4.2. $\text{CO}_2$ geological utilization

Fig. 3 presents the oil viscosity distribution over the target reservoir after 10 years of  $\text{CO}_2$ /water injection. The oil viscosity is relatively higher near the wellbores than in the main body of the target reservoir. The residual oil near the wellbores is efficiently swept by the  $\text{CO}_2$  and injected water, which causes the viscosity to become heavier due to the extraction effect of the  $\text{CO}_2$ ; that is, the  $\text{CO}_2$  has a strong extraction effect on the light hydrocarbons in the crude oil. After two cycles of  $\text{CO}_2$  extraction, the viscosity of the crude oil increases significantly. The oil viscosity over the whole target reservoir body after cycles of high-energy  $\text{CO}_2$ /water injection (case 1) is generally smaller than that after injecting  $\text{CO}_2$ /

**Table 5**

Initial mineral volume fractions and their kinetic properties [60,61].

Mineral	Vol% of solid	S ( $\text{cm}^2\cdot\text{g}^{-1}$ )	Neutral mechanism		Acid mechanism			Base mechanism		
			$k_{25}$ ( $\text{mol}\cdot(\text{m}^2\cdot\text{s})^{-1}$ )	$E_a$ ( $\text{kJ}\cdot\text{mol}^{-1}$ )	$k_{25}$ ( $\text{mol}\cdot(\text{m}^2\cdot\text{s})^{-1}$ )	$E_a$ ( $\text{kJ}\cdot\text{mol}^{-1}$ )	$n$ ( $\text{H}^+$ )	$k_{25}$ ( $\text{mol}\cdot(\text{m}^2\cdot\text{s})^{-1}$ )	$E_a$ ( $\text{kJ}\cdot\text{mol}^{-1}$ )	$n$ ( $\text{H}^+$ )
Quartz	37.83	9.800	$1.140 \times 10^{-8}$	87.70	—	—	—	—	—	—
Albite	34.84	483.000	$2.750 \times 10^{-13}$	69.80	$6.920 \times 10^{-11}$	65.0	0.457	$2.510 \times 10^{-16}$	71.0	−0.572
K-feldspar	4.56	9.800	$3.891 \times 10^{-13}$	38.00	$8.710 \times 10^{-11}$	51.7	0.500	$6.310 \times 10^{-22}$	94.1	−0.823
Calcite <sup>a</sup>	2.84	9.800	—	—	—	—	—	—	—	—
Kaolinite	0.12	151.600	$6.918 \times 10^{-14}$	22.20	$4.898 \times 10^{-12}$	65.9	0.777	$8.913 \times 10^{-18}$	17.9	−0.472
Chlorite	0.68	151.600	$3.020 \times 10^{-13}$	88.00	$7.762 \times 10^{-12}$	88.0	0.500	—	—	—
Siderite	0.09	9.800	$1.260 \times 10^{-9}$	62.76	$1.590 \times 10^{-4}$	45.0	0.900	—	—	—
Na-smectite	6.35	151.600	$1.660 \times 10^{-13}$	35.00	$1.047 \times 10^{-11}$	23.6	0.340	$3.020 \times 10^{-17}$	58.9	−0.400
Ca-smectite	6.35	151.600	$1.660 \times 10^{-13}$	35.00	$1.047 \times 10^{-11}$	23.6	0.340	$3.020 \times 10^{-17}$	58.9	−0.400
Ankerite	3.64	9.800	$1.26 \times 10^{-9}$	62.76	$1.590 \times 10^{-4}$	45.0	0.900	—	—	—
Illite	1.70	151.600	$1.660 \times 10^{-13}$	35.00	$1.047 \times 10^{-11}$	23.6	0.340	$3.020 \times 10^{-17}$	58.9	−0.400
Oligoclase	0	19.795	$1.445 \times 10^{-12}$	69.80	$2.138 \times 10^{-10}$	65.0	0.457	—	—	—
Magnetite	0	9.800	$4.571 \times 10^{-10}$	23.50	$4.169 \times 10^{-7}$	14.4	1.000	—	—	—
Dawsonite	0	9.800	$1.260 \times 10^{-9}$	62.76	$1.590 \times 10^{-4}$	45.0	0.900	—	—	—
Dolomite	0	9.800	$2.951 \times 10^{-8}$	52.20	$6.457 \times 10^{-4}$	36.1	0.500	—	—	—
Hematite	0	12.900	$2.512 \times 10^{-15}$	66.20	$4.074 \times 10^{-10}$	66.2	1.000	—	—	—

Minerals with an initial volume fraction of 0 were secondary components that may have been present during the simulation.

S: the specific reactive surface area per unit mass of solid; vol%: volume percentage of minerals to total rock skeleton.

<sup>a</sup> Calcite is controlled by local equilibrium.

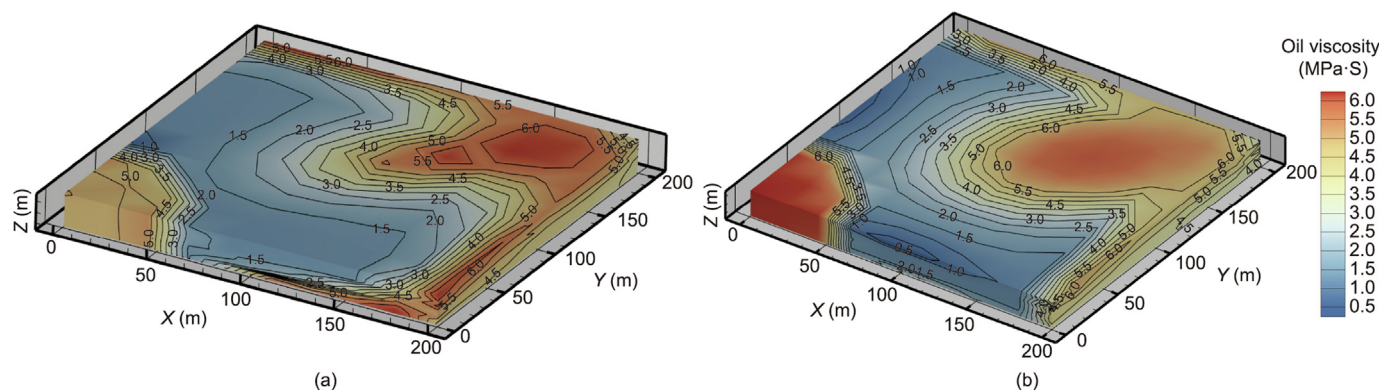


Fig. 3. Oil viscosity distributions over the target reservoir after 10 years of injection: (a) case 1 and (b) case 2.

water directly (case 2). The additional geothermal energy contributes to the viscosity reduction and facilitates  $\text{CO}_2$  utilization for enhanced oil recovery.

Fig. 4 presents the oil production in terms of the development time for high-energy  $\text{CO}_2$ /water injection (case 1) and direct  $\text{CO}_2$ /water injection (case 2). After the first four years of injection, the oil production is similar in both cases. During the initial development stage, the quantity of  $\text{CO}_2$  injected plays the key role in improving  $\text{CO}_2$  utilization and sequestration. During the 4th to 10th years of injection, the introduced geothermal energy reduces the oil viscosity and improves the mobility of the crude oil, which favors  $\text{CO}_2$  utilization. Without geothermal energy, the injected  $\text{CO}_2$ /water can readily break through due to the high mobility ratio between the crude oil and the  $\text{CO}_2$ /water. However, as the mobility ratio decreases over time due to the introduced geothermal energy, the oil production of the direct  $\text{CO}_2$ /water injection lags behind that of the high-energy  $\text{CO}_2$ /water injection. In other words, the additional geothermal energy plays a more important role in improving  $\text{CO}_2$  utilization during the 4th to 10th years of injection than during the first four years.

When the displacement efficiency in 10 years is calculated according to the sweep volume, the result is 63.6% for case 1 and 53.5% for case 2, as shown in Fig. 4. This result indicates that the main mechanism for enhancing oil recovery in case 1 is the enhanced mass transfer between the  $\text{CO}_2$  and the oil due to the high-energy injection. The averaged oil saturation (Fig. S3 in Appendix A) after the high-energy  $\text{CO}_2$ /water injection is generally lower than that after the direct  $\text{CO}_2$ /water injection, which validates the higher efficient utilization of  $\text{CO}_2$  with the assistance of geothermal energy.

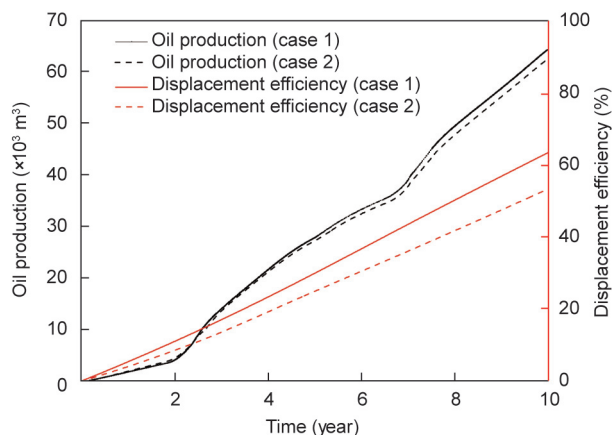


Fig. 4. Oil production and displacement efficiency in terms of development time.

#### 4.3. Energy storage and $\text{CO}_2$ sequestration during oil reservoir development

In the first 2.5 years, a relatively larger amount of  $\text{CO}_2$  dissolves into the crude oil as  $\text{CO}_2$  is injected continuously (Fig. S4 in Appendix A). As a result, the molar fraction of  $\text{CO}_2$  increases, especially near the injection wellbores, with an averaged value of 0.4485. During the 2.5–5.0-year period, water is injected, and the  $\text{CO}_2$ -saturated reservoir fluids are displaced by the injected water, which results in a sudden decrease in the molar fraction of  $\text{CO}_2$ . Subsequently,  $\text{CO}_2$  is reinjected, and the molar fraction of  $\text{CO}_2$  increases to an averaged value of 0.2209, which is less than that during the first round of  $\text{CO}_2$  injection. During the 7.5–10-year period, water is again injected, and the molar fraction of  $\text{CO}_2$  decreases to an averaged value of 0.1766. As can be seen, the injected water has a major influence on the  $\text{CO}_2$  dissolution in the reservoir fluids, which is not beneficial for  $\text{CO}_2$  sequestration.

The direct  $\text{CO}_2$ /water injection (case 2) results in relatively smaller molar fractions of  $\text{CO}_2$  in the oil phase (Figs. S4 and S5 in Appendix A). There are two main reasons for this. First, the higher temperatures in the high-energy injection scenario (case 1) keep the viscosity of the reservoir fluids at a relatively low level, which is essential for achieving sufficient contact between the  $\text{CO}_2$  and the reservoir fluids. In addition, the  $\text{CO}_2$  molecules have a higher diffusion coefficient at higher temperatures, which is critical for the miscibility between the  $\text{CO}_2$  and the reservoir fluids. Therefore, the additional geothermal energy is beneficial for  $\text{CO}_2$  sequestration in the target reservoirs. The reservoir porosity near the injection wellbore in case 1 is greater than that in case 2 (Fig. S6 in Appendix A). This finding suggests that, with the assistance of geothermal energy, the  $\text{CO}_2$ /water in case 1 exhibits better performance in flowing and sweeping the residual reservoir fluid out from the target reservoir. The resulting free space in the target reservoir is a suitable site for future large-scale  $\text{CO}_2$  sequestration and geothermal energy storage.

$\text{CO}_2$  can also be used as a suitable agent for geothermal energy storage, by transferring deep geothermal energy to a relatively shallow target reservoir for large-scale energy storage. As mentioned previously, the total energy stored in  $\text{CO}_2$  is highly dependent on the system pressure and temperature, and is composed of the temperature exergy and the pressure exergy. Fig. S2 presents the average temperature increase of the target reservoir due to the injection of high-energy  $\text{CO}_2$ /water. The reservoir pressure is greatly increased after injecting high-energy  $\text{CO}_2$ /water (Fig. S7 in Appendix A); it should be noted here that the original reservoir pressure is 15.0 MPa. The target reservoir presents a lesser pressure increase after the injection of high-energy  $\text{CO}_2$ /water (case 1) than after the direct  $\text{CO}_2$ /water injection (case 2). When

geothermal energy is transferred into the target reservoir, the viscosity of the reservoir fluids is significantly reduced, which is beneficial for the dissolution of CO<sub>2</sub> in the reservoir fluids, resulting in a relatively lower reservoir pressure.

In this simulation, CO<sub>2</sub> is injected at 43.2 t per day; after ten years of CO<sub>2</sub>/water injection, the total CO<sub>2</sub> injected is 78 840 t, and 5250 t of CO<sub>2</sub> are produced accompanied by reservoir fluids. Thus, for case 1, the effective storage quantity of CO<sub>2</sub> is 68 340 t. Similarly, in case 2, 78 840 t of CO<sub>2</sub> are injected and the quantity of CO<sub>2</sub> produced is 6750 t. Thus, for case 2, the effective storage quantity of CO<sub>2</sub> is 65 340 t. According to Eq. (3), the geothermal energy stored in the CO<sub>2</sub> in case 1 can be calculated to be around  $2.10 \times 10^4$  GJ. (The CO<sub>2</sub> in case 2 is not considered to store geothermal energy in this work.) In order to improve the storage capacity of geothermal energy and CO<sub>2</sub> sequestration in the target geological reservoir body, the target oil reservoir is deemed to be depleted at this point, and five more injection wells are built for CO<sub>2</sub> injection (Section 4.4).

#### 4.4. Energy storage and CO<sub>2</sub> sequestration in a geological oil reservoir body

Based on the geological background of Block H59 in Jilin Oil-field, China [40], a 1:1 3D numerical model was established, as shown in Fig. 5. According to the existing well deployment, six injection wells are opened for CO<sub>2</sub> injection in the model. This model is employed to assess the potential of the site sequestration

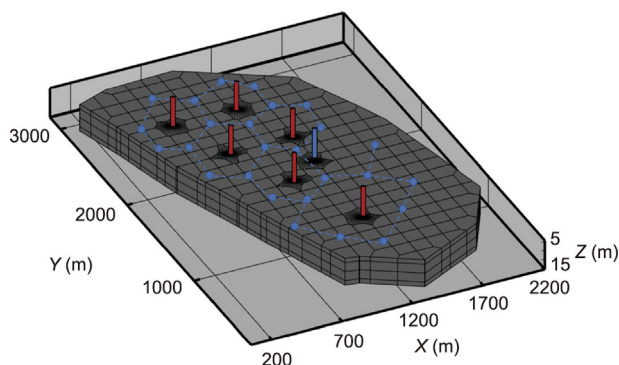


Fig. 5. Concept model of the oil reservoir site for sequestration and energy storage-potential assessment.

and energy storage capacity of CO<sub>2</sub>. The heat extraction rate gradually decreases as the injection time increases (Fig. S8 in Appendix A), indicating that, as more CO<sub>2</sub> is injected into the target reservoir over time, the temperature of the CO<sub>2</sub> decreases. Therefore, the heat extraction process is stopped after 30 years of CO<sub>2</sub> injection through the geothermal layer, considering the low efficiency of heat extraction. After 30 years, CO<sub>2</sub> is injected directly into the target oil reservoir for another 80 years for CO<sub>2</sub> sequestration.

After 10 years of oil reservoir development (i.e., water injection alternating with CO<sub>2</sub> injection), CO<sub>2</sub> is then injected for 100 years for CO<sub>2</sub> sequestration and energy storage, until more than 90% of the total porosity of the entire site is occupied. Fig. 6 presents the spatial distribution of the CO<sub>2</sub> after 110 years at different reservoir depths. Due to its buoyancy, CO<sub>2</sub> accumulates in large quantities at the top of the oil reservoir geological body. In order to improve the utilization efficiency of the oil reservoir geological body, six injection wells are opened for CO<sub>2</sub> injection after 10 years' oil production. Fig. 7 presents the utilization efficiency of the reservoir geological body and the corresponding total quantity of CO<sub>2</sub> injection. It is found that the utilization efficiency of the geological body increases as more CO<sub>2</sub> is injected. The final quantity of CO<sub>2</sub> injection at the site is as high as  $9.529 \times 10^8$  t, at which the utilization efficiency of the geological body is up to 91.2%.

In addition to CO<sub>2</sub> sequestration, the CO<sub>2</sub> is employed as an excellent medium for geothermal energy storage. According to Eq. (3), the total energy stored in the target geological reservoir body is calculated in terms of the injection time. Fig. 8 presents the geothermal energy stored in the target geological reservoir body as CO<sub>2</sub> is injected. It can be seen that the energy stored is transformed into a standard coal mass in Fig. 8. The calorific value of standard coal is  $2.933 \times 10^4$  kJ·kg<sup>-1</sup>, which is a method for representing standard energy. We find that the geothermal energy stored by CO<sub>2</sub> increases linearly as more CO<sub>2</sub> is injected and sequestered in the target geological reservoir body. The geothermal energy stored through CO<sub>2</sub> is as much as  $2.46 \times 10^8$  GJ after 100 years of CO<sub>2</sub> injection. If it is assumed that the general energy consumption of a normal household is around 7.0 GJ·a<sup>-1</sup>, then the energy stored through CO<sub>2</sub> could provide the yearly energy supply for over  $3.5 \times 10^7$  normal households. Therefore, a substantial amount of geothermal energy stored through CO<sub>2</sub> can be meaningful for a future energy supply. In addition, the integrated approach well combines geothermal energy storage with CO<sub>2</sub> sequestration and utilization, and its wide application holds great significance for both large-scale geothermal energy storage and the achievement of future carbon neutrality goals.

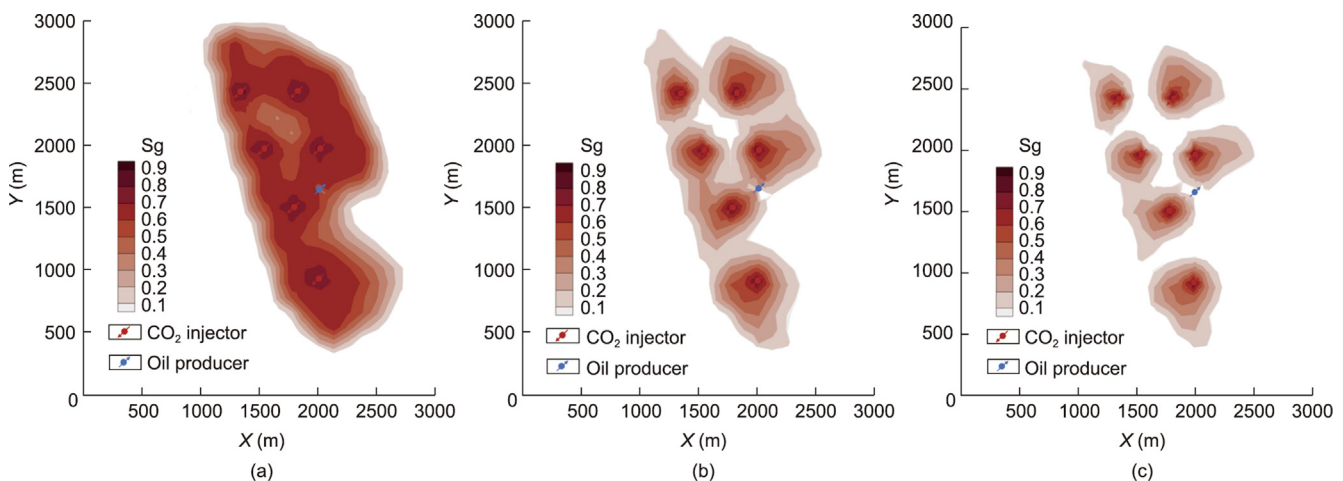


Fig. 6. Spatial distribution of CO<sub>2</sub> in 110 years at different reservoir depths. (a) –1500 m; (b) –1505 m; (c) –1520 m. Sg: the saturation of CO<sub>2</sub>.



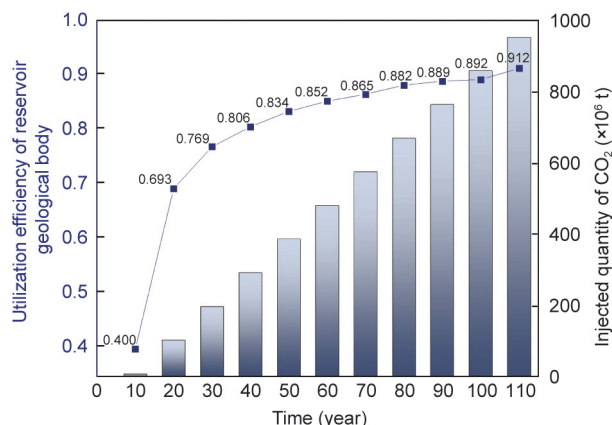


Fig. 7. Utilization efficiency of the reservoir geological body and its corresponding total quantity of CO<sub>2</sub> injection.

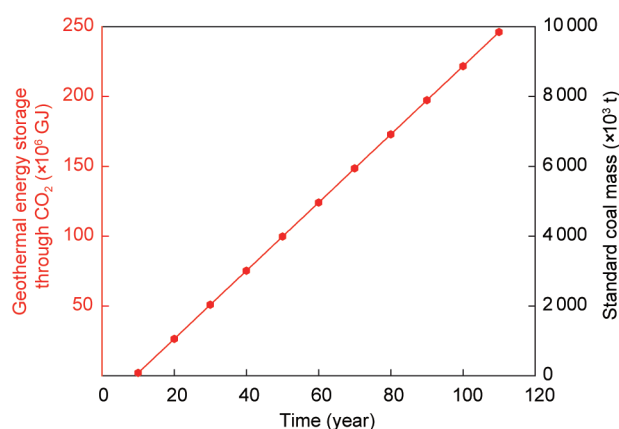


Fig. 8. Geothermal energy stored in the target geological reservoir body as CO<sub>2</sub> is injected.

In order to evaluate the security of CO<sub>2</sub> sequestration in the target geological oil reservoir body, we quantitatively investigated the phase transitions of CO<sub>2</sub> in the next 1000 years when sequestered in the target reservoir, as shown in Fig. 9. More specifically, the proportion of CO<sub>2</sub> in each phase—that is, the CO<sub>2</sub> dissolved in the oil phase, water phase, gas phase (supercritical), and mineralized phase—is calculated in terms of the sequestered time. The CO<sub>2</sub> in the target oil reservoir body mainly exists as supercritical CO<sub>2</sub>, accounting for up to 70% of the total CO<sub>2</sub>; this is followed in order by CO<sub>2</sub> in the liquid phase and then CO<sub>2</sub> in the mineralized phase. The amount of CO<sub>2</sub> dissolved in the oil phase is greater than that in the water phase; in other words, in the geological oil reservoir body, CO<sub>2</sub> tends to dissolve into the oil phase rather than the water phase for sequestration. As the sequestration process continues, the quantity of CO<sub>2</sub> dissolved in the aqueous phase increases as the CO<sub>2</sub> is further transformed into carbonate minerals, of which there are up to around  $7.2 \times 10^5$  t after 1000 years' sequestration. Thus, the total amount of gaseous CO<sub>2</sub> decreases. In comparison, the total amount of CO<sub>2</sub> dissolved in the oil phase remains basically unchanged.

## 5. Conclusions

This work proposed an integrated framework for synergistic geothermal energy storage, carbon sequestration, and CO<sub>2</sub> utilization. The key conclusions are summarized as follows:

- (1) When injected through the geothermal layer, CO<sub>2</sub> is heated to an average temperature of 341.75 K. After the injection of high-energy CO<sub>2</sub> for 2.5 years, the average temperatures of the target reservoir increase by around 276.15 K, and the average pressure of the target reservoir increases to 25.1–47.7 MPa, which is beneficial for efficient CO<sub>2</sub> utilization and geothermal energy storage.
- (2) By introducing geothermal energy into the target reservoir, the solubility of CO<sub>2</sub> in the reservoir fluids is greatly improved. The injection of high-energy CO<sub>2</sub>/water exhibits a better performance

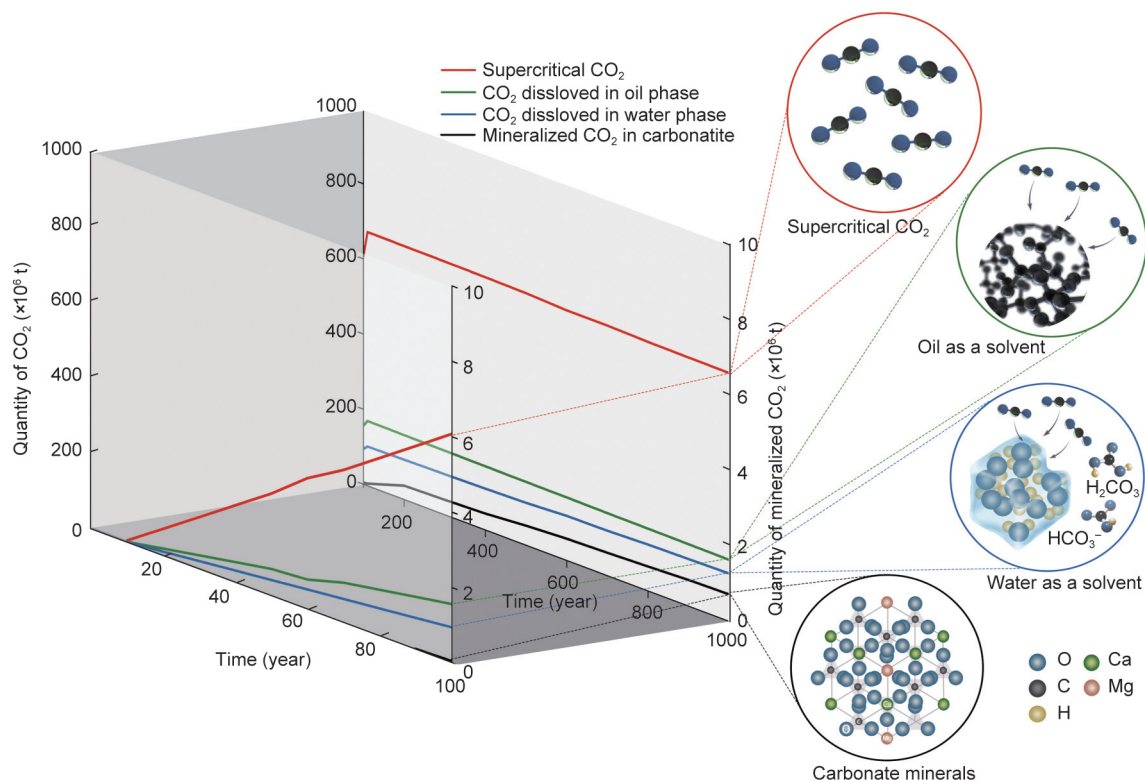


Fig. 9. Phase transitions of CO<sub>2</sub> in the target geological reservoir body over the next 1000 years.

than the direct injection of CO<sub>2</sub>/water in sweeping the reservoir fluids out from the pore and throat, due to the introduction of the geothermal energy. Hence, the free space in the target reservoir becomes a suitable site for future large-scale CO<sub>2</sub> sequestration and geothermal energy storage.

(3) When CO<sub>2</sub> is injected for 110 years, the utilization efficiency of the geological body reaches 91.2% and the final injection quantity of CO<sub>2</sub> in the site is as high as  $9.529 \times 10^8$  t. After 1000 years of sequestration, CO<sub>2</sub> mainly exists in the form of supercritical CO<sub>2</sub>, which accounts for up to 70% of the total CO<sub>2</sub>; this is followed in order by CO<sub>2</sub> in the liquid phase and then CO<sub>2</sub> in the mineralized phase. Moreover, the amount of CO<sub>2</sub> dissolved in the oil phase is greater than that in the water phase; in other words, CO<sub>2</sub> sequestration accounting for dissolution trapping increases significantly due to the presence of residual oil.

(4) CO<sub>2</sub> can be employed as a suitable medium for geothermal energy storage, as it can extract heat from deep geothermal layers and then be used to efficiently store the extracted heat in the target reservoir. As much as  $2.46 \times 10^8$  GJ of geothermal energy can be stored in the CO<sub>2</sub> after 100 years of CO<sub>2</sub> injection, which could provide a yearly energy supply for over  $35 \times 10^6$  normal households. This degree of large-scale energy storage is of great significance for providing a future large-scale supply of geothermal energy.

(5) The integrated approach synergistically combines geothermal energy storage with CO<sub>2</sub> sequestration and utilization, which is of great significance for large-scale geothermal energy storage in the future; in addition, the combined approach is beneficial for achieving the goal of carbon neutrality.

## Acknowledgments

This work is supported by the National Key Research and Development Program of China under grant (2022YFE0206700). We also acknowledge the financial support by the National Natural Science Foundation of China (52004320), and the Science Foundation of China University of Petroleum, Beijing (2462021QNXZ012 and 2462021YJRC012).

## Compliance with ethics guidelines

Yueliang Liu, Ting Hu, Zhenhua Rui, Zheng Zhang, Kai Du, Tao Yang, Birol Dindoruk, Erling Halfdan Stenby, Farshid Torabi, and Andrey Afanasyev declare that they have no conflict of interest or financial conflicts to disclose.

## Appendix A. Supplementary data

Supplementary data to this article can be found online at <https://doi.org/10.1016/j.eng.2022.12.010>.

## References

- [1] Goeppert A, Czaun M, May RB, Prakash GKS, Olah GA, Narayanan SR. Carbon dioxide capture from the air using a polyamine based regenerable solid adsorbent. *J Am Chem Soc* 2011;133(50):20164–7.
- [2] International Energy Agency (IEA). Global energy review: CO<sub>2</sub> emissions in 2021. Report. Paris: International Energy Agency; 2021.
- [3] Brown DW. A hot dry rock geothermal energy concept utilizing supercritical CO<sub>2</sub> instead of water. In: Proceedings of the Twenty-Fifth Workshop on Geothermal Reservoir Engineering; 2000 Jan 24–26; Stanford, CA, USA. Stanford: Stanford Geothermal Program Workshop; 2000. p. 1–6.
- [4] Pruess K. Enhanced geothermal systems (EGS) using CO<sub>2</sub> as working fluid—a novel approach for generating renewable energy with simultaneous sequestration of carbon. *Geothermics* 2006;35(4):351–67.
- [5] Pruess K. On production behavior of enhanced geothermal systems with CO<sub>2</sub> as working fluid. *Energy Convers Manage* 2008;49(6):1446–54.
- [6] Atrens AD, Gurgenci H, Rudolph V. CO<sub>2</sub> thermosiphon for competitive geothermal power generation. *Energy Fuels* 2009;23(1):553–7.
- [7] Atrens AD, Gurgenci H, Rudolph V. Electricity generation using a carbon-dioxide thermosiphon. *Geothermics* 2010;39(2):161–9.
- [8] Adams BM, Kuehn TH, Bielicki JM, Randolph JB, Saar MO. A comparison of electric power output of CO<sub>2</sub> plume geothermal (CPG) and brine geothermal systems for varying reservoir conditions. *Appl Energy* 2015;140:365–77.
- [9] Randolph JB, Adams BM, Kuehn TH, Saar MO. Wellbore heat transfer in CO<sub>2</sub>-based geothermal systems. *Trans Geotherm Resour Coun* 2012;36:546–54.
- [10] Pruess K. Enhanced geothermal systems (EGS): comparing water and CO<sub>2</sub> as heat transmission fluids. In: Proceedings of the New Zealand Geothermal Workshop; 2006 Nov 28; Auckland, New Zealand. Auckland: Geothermal Association; 2007. p. 1–13.
- [11] Randolph JB, Saar MO. Combining geothermal energy capture with geologic carbon dioxide sequestration. *Geophys Res Lett* 2011;38(10):L10401.
- [12] Randolph JB, Saar MO. Impact of reservoir permeability on the choice of subsurface geothermal heat exchange fluid: CO<sub>2</sub> versus water and native brine. *Trans Geotherm Resour Coun* 2011;35:521–6.
- [13] Liu Y, Hou J. Selective adsorption of CO<sub>2</sub>/CH<sub>4</sub> mixture on clay-rich shale using molecular simulations. *J CO<sub>2</sub> Util* 2020;39:101143.
- [14] Bielicki JM, Pollak MF, Fitts JP, Peters CA, Wilson EJ. Causes and financial consequences of geologic CO<sub>2</sub> storage reservoir leakage and interference with other subsurface resources. *Int J Greenh Gas Control* 2014;20:272–84.
- [15] Bielicki JM, Peters CA, Fitts JP, Wilson EJ. An examination of geologic carbon sequestration policies in the context of leakage potential. *Int J Greenh Gas Control* 2015;37:61–75.
- [16] Bielicki JM, Pollak MF, Deng H, Wilson EJ, Fitts JP, Peters CA. The leakage risk monetization model for geologic CO<sub>2</sub> storage. *Environ Sci Technol* 2016;50(10):4923–31.
- [17] Gibbins J, Chalmers H. Carbon capture and storage. *Energy Policy* 2008;36(12):4317–22.
- [18] Ezekiel J, Ebigo A, Adams BM, Saar MO. Combining natural gas recovery and CO<sub>2</sub>-based geothermal energy extraction for electric power generation. *Appl Energy* 2020;269:115012.
- [19] Hefny M, Qin CZ, Saar MO, Ebigo A. Synchrotron-based pore-network modeling of two-phase flow in Nubian Sandstone and implications for capillary trapping of carbon dioxide. *Int J Greenh Gas Control* 2020;103:103164.
- [20] Fleming MR, Adams BM, Ogland-Hand JD, Bielicki JM, Kuehn TH, Saar MO. Flexible CO<sub>2</sub>-plume geothermal (CPG-F): using geologically stored CO<sub>2</sub> to provide dispatchable power and energy storage. *Energy Convers Manage* 2022;253:115082.
- [21] Intergovernmental Panel on Climate Change (IPCC). Special report on carbon dioxide capture and storage. Report. Cambridge: Cambridge University Press; 2005.
- [22] Presser D, Cafaro VG, Cafaro D. Optimal sourcing, supply and development of carbon dioxide networks for enhanced oil recovery in CCUS systems. *Computer-Aided Chem Eng* 2022;49:493–8.
- [23] Ampomah W, Balch RS, Cather M, Will R, Gunda D, Dai Z, et al. Optimum design of CO<sub>2</sub> storage and oil recovery under geological uncertainty. *Appl Energy* 2017;195:80–92.
- [24] Jia W, McPherson B, Pan F, Dai Z, Xiao T. Uncertainty quantification of CO<sub>2</sub> storage using Bayesian model averaging and polynomial chaos expansion. *Int J Greenh Gas Control* 2018;71:104–15.
- [25] Keating E, Bacon D, Carroll S, Mansoor K, Sun Y, Zheng L, et al. Applicability of aquifer impact models to support decisions at CO<sub>2</sub> sequestration sites. *Int J Greenh Gas Control* 2016;52:319–30.
- [26] Jiang J, Rui Z, Hazlett R, Lu J. An integrated technical-economic model for evaluating CO<sub>2</sub> enhanced oil recovery development. *Appl Energy* 2019;247:190–211.
- [27] Chaturvedi KR, Sharma T. *In-situ* formulation of pickering CO<sub>2</sub> foam for enhanced oil recovery and improved carbon storage in sandstone formation. *Chem Eng Sci* 2021;235:116484.
- [28] Rezk MG, Foroozesh J, Zivar D, Mumtaz M. CO<sub>2</sub> storage potential during CO<sub>2</sub> enhanced oil recovery in sandstone reservoirs. *J Nat Gas Sci Eng* 2019;66:233–43.
- [29] Gu Y, Zhang S, She Y. Effects of polymers as direct CO<sub>2</sub> thickeners on the mutual interactions between a light crude oil and CO<sub>2</sub>. *J Polym Res* 2013;20(2):61.
- [30] Pan F, McPherson BJ, Dai Z, Jia W, Lee SY, Ampomah W, et al. Uncertainty analysis of carbon sequestration in an active CO<sub>2</sub>-EOR field. *Int J Greenh Gas Control* 2016;51:18–28.
- [31] Davarpanah A, Mirshekari B. Experimental study of CO<sub>2</sub> solubility on the oil recovery enhancement of heavy oil reservoirs. *J Therm Anal Calorim* 2020;139(2):1161–9.
- [32] Liu Y, Li H, Okuno R. Measurements and modeling of interfacial tension of CO<sub>2</sub>–CH<sub>4</sub>–brine system at reservoir conditions. *Ind Eng Chem Res* 2016;55(48):12358–75.
- [33] Kong S, Feng G, Liu Y, Li K. Potential of dimethyl ether as an additive in CO<sub>2</sub> for shale oil recovery. *Fuel* 2021;296:120643.
- [34] Huang X, Li A, Li X, Liu Y. Influence of typical core minerals on tight oil recovery during CO<sub>2</sub> flooding using the nuclear magnetic resonance technique. *Energy Fuels* 2019;33(8):7147–54.
- [35] Azzolina NA, Nakles DV, Gorecki CD, Peck WD, Ayash SC, Melzer LS, et al. CO<sub>2</sub> storage associated with CO<sub>2</sub> enhanced oil recovery: a statistical analysis of historical operations. *Int J Greenh Gas Control* 2015;37:384–97.
- [36] Aminu MD, Nabavi SA, Rochelle CA, Manovic V. A review of developments in carbon dioxide storage. *Appl Energy* 2017;208:1389–419.
- [37] Bachu S. Identification of oil reservoirs suitable for CO<sub>2</sub>-EOR and CO<sub>2</sub> storage (CCUS) using reserves databases, with application to Alberta, Canada. *Int J Greenh Gas Control* 2016;44:152–65.

- [38] Yang W, Peng B, Liu Q, Wang S, Dong Y, Lai Y. Evaluation of CO<sub>2</sub> enhanced oil recovery and CO<sub>2</sub> storage potential in oil reservoirs of Bohai Bay Basin. *China Int J Greenh Gas Control* 2017;65:86–98.
- [39] Ahmed T. Minimum miscibility pressure from EOS. In: Proceedings of Canadian International Petroleum Conference; 2000 Jun 4–8; Calgary, AB, Canada. Calgary: Petroleum Society of Canada; 2000.
- [40] Ren B, Ren S, Zhang L, Chen G, Zhang H. Monitoring on CO<sub>2</sub> migration in a tight oil reservoir during CCS-EOR in Jilin Oilfield China. *Energy* 2016;98:108–21.
- [41] Rommerskirchen R, Nijssen P, Bilgili H, Sottmann T. Additives for CO<sub>2</sub> EOR applications. In: Proceedings of Annual Technical Conference and Exhibition (ACTE); 2016 Sep 26–28; Dubai, United Arab Emirates. Dubai: Society of Petroleum Engineers; 2016.
- [42] Liu Y, Rui Z. A storage-driven CO<sub>2</sub> EOR for net-zero emission target. *Engineering* 2022;18(11):79–87.
- [43] Liu Y, Rui Z, Yang T, Dindoruk B. Using propanol as an additive to CO<sub>2</sub> for improving CO<sub>2</sub> utilization and storage in oil reservoirs. *Appl Energy* 2022;311:118640.
- [44] Salehi MM, Safarzadeh MA, Sahraei E, Nejad SAT. Comparison of oil removal in surfactant alternating gas with water alternating gas, water flooding and gas flooding in secondary oil recovery process. *J Petrol Sci Eng* 2014;120:86–93.
- [45] Dai Z, Middleton R, Viswanathan H, Fessenden-Rahn J, Bauman J, Pawar R, et al. An integrated framework for optimizing CO<sub>2</sub> sequestration and enhanced oil recovery. *Environ Sci Technol Lett* 2014;1(1):49–54.
- [46] Adebayo AR, Kamal MS, Barri AA. An experimental study of gas sequestration efficiency using water alternating gas and surfactant alternating gas methods. *J Nat Gas Sci Eng* 2017;42:23–30.
- [47] Zhao X, Liao X, Wang W, Chen C, Liao C, Rui Z. Estimation of CO<sub>2</sub> storage capacity in oil reservoir after waterflooding: case studies in Xinjiang Oilfield from west China. *Adv Mat Res* 2013;734–7:1183–8.
- [48] Zhao X, Liao X, Wang W, Chen C, Rui Z, Wang H. The CO<sub>2</sub> storage capacity evaluation: methodology and determination of key factors. *J Energy Inst* 2014;87(4):297–305.
- [49] Zhao X, Rui Z, Liao X. Case studies on the CO<sub>2</sub> storage and EOR. In heterogeneous, highly water-saturated, and extra-low permeability Chinese reservoir. *J Nat Gas Sci Eng* 2016;29:275–83.
- [50] Xu T, Li J. Reactive transport modeling to address the issue of CO<sub>2</sub> geological sequestration. *Procedia Earth Planet Sci* 2013;7:912–5.
- [51] Xu T, Apps JA, Pruess K. Numerical simulation of CO<sub>2</sub> disposal by mineral trapping in deep aquifers. *Appl Geochem* 2004;19(6):917–36.
- [52] Oldenburg CM, Pan L. TOGA: A TOUGH code for modeling three-phase, multicomponent, and non-isothermal processes involved in CO<sub>2</sub>-based enhanced oil recovery. Report. Berkeley: Lawrence Berkeley National Laboratory; 2019.
- [53] Yeh G, Tripathi S. A model for simulating transport of reactive multispecies components: model development and demonstration. *Water Resour Res* 1991;27(12):3075–94.
- [54] Hu T. Study on the process model of CO<sub>2</sub> migration and phase transformation in enhanced oil recovery system [dissertation]. Changchun: Jilin University; 2022. Chinese.
- [55] Pan L, Oldenburg CM. T2Well—an integrated wellbore-reservoir simulator. *Comput Geosci* 2014;65:46–55.
- [56] Ramey HJ. Wellbore heat transmission. *J Pet Technol* 1962;14(04):427–35.
- [57] Guo X, Du Z, Sun L, Fu Y, Huang W, Zhang C. Optimization of tertiary water-alternate-CO<sub>2</sub> flood in Jilin oil field of China: laboratory and simulation studies. In: Proceedings of SPE/DOE Symposium on Improved Oil Recovery; 2006 Apr 22–26; Tulsa, OK, USA. Richardson: OnePetro; 2006. p. SPE-99616-MS.
- [58] Hu Z, Xu T, Feng B, Yuan Y, Li F, Feng G, et al. Thermal and fluid processes in a closed-loop geothermal system using CO<sub>2</sub> as a working fluid. *Renew Energy* 2020;154:351–67.
- [59] Lei H. Deposition mechanisms and reservoir protection countermeasures of a low-permeability formation in CO<sub>2</sub> flooding process [dissertation]. Beijing: China University of Petroleum; 2017. Chinese.
- [60] Zhang L, Li X, Ren B, Cui G, Zhang Y, Ren S, et al. CO<sub>2</sub> storage potential and trapping mechanisms in the H-59 block of Jilin Oilfield China. *Int J Greenh Gas Control* 2016;49:267–80.
- [61] Tian H, Pan F, Xu T, McPherson BJ, Yue G, Mandalaparty P. Impacts of hydrological heterogeneities on caprock mineral alteration and containment of CO<sub>2</sub> in geological storage sites. *Int J Greenh Gas Control* 2014;24:30–42.
- [62] Quiñones-Cisneros SE, Zéberg-Mikkelsen CK, Stenby EH. The friction theory (f-theory) for viscosity modeling. *Fluid Phase Equilib* 2000;169(2):249–76.
- [63] Aprhornratana S, Eames IW. Thermodynamic analysis of absorption refrigeration cycles using the second law of thermodynamics method. *Int J Refrig* 1995;18(4):244–52.
- [64] Vidal A, Best R, Rivero R, Cervantes J. Analysis of a combined power and refrigeration cycle by the exergy method. *Energy* 2006;31(15):3401–14.